Periodic steady vortices in a stagnation-point flow

By OLIVER S. KERR† AND J. W. DOLD

School of Mathematics, University of Bristol, Bristol BS8 4TW, UK

A stagnation point flow of the form $U = (0, Ay, -Az)$ is unstable to three-dimensional disturbances. It has been shown that the vorticity components of such a disturbance that are perpendicular to the direction of the diverging flow will decay, and that the parallel component of vorticity can grow. We augment these findings by showing that fully nonlinear steady-state deviations from this flow exist that consist of a periodic distribution of counter-rotating vortices whose axes lie parallel to the direction of the diverging flow. These solutions have two independent parameters: the dimensionless strength of the converging flow, and the intensity of the vortices. We examine the structure of these vortices in the asymptotic limits of large strain rate of the converging flow, and of large amplitude of the vortices.

1. Introduction

In this paper we look at three-dimensional steady perturbations (which need not be small) to a steady two-dimensional stagnation point flow, or extensional flow, of the form $U = (0, Ay, -Az)$ with $A > 0$. Originally motivated by a desire for a simple model of mixing between converging streams of gases, we considered the possible existence of steady-state solutions to the Navier–Stokes equation that are perturbations to this stagnation-point flow. With this geometry it is easy to show that any nonlinear perturbation to this stagnation-point flow that initially has no y-dependence will retain this property throughout its evolution. We exploit this feature by looking for solutions to the steady problem that consist of perturbations with no y-dependence. We find solutions to the governing equations that consist of a periodic row of steady counter-rotating vortices, with axes parallel to the y-axis. The vortices found are reminiscent of the vortex in an axisymmetric converging flow found by Burgers (1948). In both cases the persistent state of the vortices is due to a balance between the intensification of the vorticity due to the stretching of the vortex lines by the diverging flow parallel to the vortex axes, and the dissipation of the vorticity due to viscosity. As with the Burgers vortex the vortices found here can have arbitrary strength.

Although this problem was initially investigated as a theoretical exercise, the flows found do have application to real fluid flow phenomena. The undisturbed background flow considered here is good approximation to the flow in a 'four-roll mill' used by Taylor (1934) in his study of droplet breakup. The stability of this two-dimensional flow has received little theoretical attention. Pearson (1959) found that, in the context of homogeneous turbulence, the extensional flow was always unstable. Aryshev, Golovin & Ershin (1981) looked at the linear stability of an inviscid fluid in such a regime, while Lagnado, Phan-Thien & Leal (1984), as a special case in their investigation of the stability of general two-dimensional linear flows, found an explicit expression for the temporal and spatial evolution of an arbitrary linear disturbance to

† Current address: Department of Mathematics, City University, Northampton Square, London EC1V 0HB, UK.

the vorticity in such a stagnation-point flow. In addition, Lin & Corcos (1984) found a similarity solution that described a set of decaying linear disturbances to this stagnation-point flow which allowed for a time-dependent strain rate, A. Lagnado & Leal (1990) investigated experimentally the three-dimensional disturbances that appeared in the extensional flow found in a 'four-roll mill' when the strain rate was sufficiently large. These disturbances first manifest themselves as a steady vortex in the centre of the mill, whose axis is aligned with the direction of the diverging flow. These instabilities closely resemble the vortices found in this work. For larger strain rates the flows in the experiments became time dependent.

Another area in which there has been a significant interest in disturbances to stagnation-point flows has been in the context of the evolution of instabilities between two bodies of fluid separated by a shear layer. The primary Kelvin–Helmholtz instabilities to this flow takes the form of co-rotating vortices lying in the plane of the shear layer, with their axes perpendicular to the flow. As the amplitude of these vortices grows, a secondary instability occurs that takes the form of counter-rotating vortices aligned approximately with the main flow direction, and lying between the transverse vortices. These secondary instabilities have been studied both numerically and experimentally by several authors (see, for example, Corcos & Lin 1984; Knio & Ghoniem 1992; Lasheras, Cho & Maxworthy 1986; Lasheras & Choi 1988; Lin & Corcos 1984; Meiburg & Lasheras 1988; Metcalfe *et al.* 1987; Moser & Rogers 1991; Neu 1984). These longitudinal secondary vortices lie in a region where the flow is approximately that of the two-dimensional stagnation-point flow considered here. In this context the time-dependent behaviour of vortices in such flows has received particular attention from Lin & Corcos (1984) and Neu (1984).

The equations governing these vortices in a stagnation-point flow are derived in §2 and some solutions are presented in §3. The asymptotic forms of the solutions for large strain rates in the converging flow and for large amplitudes of the vortices are given in §4 and §5 respectively.

2. The governing equations

We consider the situation where the full flow consists of perturbations to the steady stagnation-point flow

$$U(x, y, z) = (0, Ay, -Az) \tag{1}$$

with $A > 0$. The fully nonlinear, time-independent velocity and pressure perturbations, u and p, to this flow will satisfy

$$u \cdot \nabla u + U \cdot \nabla u + u \cdot \nabla U = -\frac{1}{\rho} \nabla p + \nu \nabla^2 u, \tag{2}$$

with

$$\nabla \cdot u = 0, \tag{3}$$

where ρ is the density of the fluid, and ν the kinematic viscosity.

By looking for perturbations to the stagnation-point flow that are independent of the y-coordinate, and have no perturbation velocity component in this direction, (2) simplifies to

$$\left(u \frac{\partial}{\partial x} + w \frac{\partial}{\partial z}\right) u - Az \frac{\partial u}{\partial z} - wA\hat{z} = -\frac{1}{\rho} \nabla p + \nu \left(\frac{\partial^2}{\partial x^2} + \frac{\partial^2}{\partial z^2}\right) u \tag{4}$$

and

$$\frac{\partial u}{\partial x} + \frac{\partial w}{\partial z} = 0. \tag{5}$$

If we use a stream function $\psi(x, z)$ such that

$$\boldsymbol{u} = (u, 0, w) = \left(-\frac{\partial \psi}{\partial z}, 0, \frac{\partial \psi}{\partial x}\right), \tag{6}$$

then the continuity equation will be satisfied, and (4) becomes

$$-\frac{\partial \psi}{\partial z}\frac{\partial \omega}{\partial x} + \frac{\partial \psi}{\partial x}\frac{\partial \omega}{\partial z} - Az\frac{\partial \omega}{\partial z} - A\omega = \nu\left(\frac{\partial^2}{\partial x^2} + \frac{\partial^2}{\partial z^2}\right)\omega, \tag{7}$$

where the vorticity, ω, is given by

$$\omega = -\left(\frac{\partial^2}{\partial x^2} + \frac{\partial^2}{\partial z^2}\right)\psi. \tag{8}$$

If we look for solutions that are periodic in the x-direction, with period $2\pi/k$, we can non-dimensionalize this equation, using k^{-1} as a lengthscale, and ν as a scale for ψ, yielding

$$-\frac{\partial \psi^*}{\partial z^*}\frac{\partial \omega^*}{\partial x^*} + \frac{\partial \psi^*}{\partial x^*}\frac{\partial \omega^*}{\partial z^*} - \lambda z^*\frac{\partial \omega^*}{\partial z^*} - \lambda\omega^* = \left(\frac{\partial^2}{\partial x^{*2}} + \frac{\partial^2}{\partial z^{*2}}\right)\omega^*, \tag{9}$$

$$\omega^* = -\left(\frac{\partial^2}{\partial x^{*2}} + \frac{\partial^2}{\partial z^{*2}}\right)\psi^*, \tag{10}$$

where the superscripts * indicate non-dimensional quantities. These superscripts will be dropped henceforth.

Here

$$\lambda = \frac{A}{\nu k^2} \tag{11}$$

is a non-dimensional measure of the strength of the converging flow compared to the rate of viscous dissipation. An alternative interpretation of this parameter is that it is the square of the ratio of the vortex separation to the thickness of the viscous layer associated with a stagnation-point flow (Burgers, 1948). However, for simplicity we will refer to it here in terms of being a measure of the flow strength.

To find solutions we exploit the periodicity by expanding ω and ψ in Fourier series in x:

$$\omega(x, z) = \sum_{n=1}^{\infty} a_n(z)\cos(2n-1)x + b_n(z)\sin 2nx, \tag{12}$$

$$\psi(x, z) = \sum_{n=1}^{\infty} c_n(z)\cos(2n-1)x + d_n(z)\sin 2nx. \tag{13}$$

These expansions can be substituted in to the governing equations and the coefficients of the various Fourier modes collected to given an infinite system of ordinary differential equations

$$a_n'' + \lambda z a_n' + (\lambda - (2n-1)^2)a_n = J_{2n-1}(\psi, \omega), \tag{14}$$

$$b_n'' + \lambda z b_n' + (\lambda - 4n^2)b_n = J_{2n}(\psi, \omega), \tag{15}$$

$$c_n'' - (2n-1)^2 c_n = -a_n, \tag{16}$$

$$d_n'' - 4n^2 d_n = -b_n, \tag{17}$$

where $J_{2n-1}(\psi, \omega)$ and $J_{2n}(\psi, \omega)$ are the appropriate components of the nonlinear terms. The symmetry of the expected solutions,

$$\psi(x, z) = \psi(-x, -z) \quad \text{and} \quad \psi(x, z) = -\psi(\pi - x, z), \tag{18}$$

tells us that each $a_n(z)$ is an even function, and each $b_n(z)$ is an odd function in z. Hence, when looking for solutions, we can impose the boundary conditions

$$a'_n(0) = b_n(0) = c'_n(0) = d_n(0) = 0, \tag{19}$$

$$a_n \to 0, b_n \to 0, c_n \to 0 \quad \text{and} \quad d_n \to 0 \quad \text{as} \quad z \to \infty, \tag{20}$$

on each a_n, b_n, c_n and d_n, and we need only solve for $z \geqslant 0$.

3. Structure of the vortices

The nature of small-amplitude disturbances can be found by linearizing the governing equations. Examination of the linearized vorticity equation for the fundamental mode

$$a''_1 + \lambda z a'_1 + (\lambda - 1) a_1 = 0 \tag{21}$$

shows us that for $\lambda < 1$ there are no positive maxima nor negative minima, hence the only possible solution for this equation that decays as $z \to \pm \infty$ is the trivial solution $a_1(z) \equiv 0$. When $\lambda = 1$ equation (21) can be solved explicitly, and again the only solution that decays to 0 as $z \to \pm \infty$ is the trivial solution. In this particular case it is of interest to notice that the full equations (9) and (10) admit the solution

$$\psi = \omega = \cos x. \tag{22}$$

This is the solution found by Craik & Criminale (1986) as a special case in their examination of the stability of disturbances that consist of single Fourier modes in unbounded shear flows. For $\lambda > 1$ it can be shown that all solutions to this linearized equation for $a_1(z)$ decay as $z \to \pm \infty$. Hence the condition that $\lambda > 1$ is a necessary and sufficient condition for the existence of linear non-trivial solutions that decay in the far field.

In the linearized problem, any functions $a_n(z)$ and $b_n(z)$ that satisfy the far-field boundary conditions will be identically zero for $\lambda \leqslant (2n-1)^2$ and $\lambda \leqslant 4n^2$ respectively. The linearity allows solutions that are linear combinations of any non-zero modes found for $\lambda > 1$.

As will be seen below, the nature of a single mode of the linear disturbances is not intrinsically different from the nonlinear disturbances. The structure of the perturbations is found to vary slowly as the amplitude is increased from infinitesimal to large values, with no abrupt or significant changes in its form. Hence we will not examine the linear solutions in any detail in this section.

The criterion that $\lambda > 1$ for non-trivial solutions to exist differs from the situation with the axisymmetric single vortex of Burgers (1948), for which solutions can exist for any strain rate. In both cases as the strain rate decreases so the enhancement of the vorticity by vortex stretching decreases. For a balance to occur between the enhancement of vorticity and viscous dissipation the dissipation rate must also decrease. This requires that the dissipation occurs over an ever increasing lengthscale. For the Burgers vortex this is possible as the diameter of the vortex can increase without bound. For the periodic vortices the distance between adjacent vortices provides an upper limit for the lengthscale of the dissipation, and hence gives a lower limit to the dissipation rate. This dissipation must be overcome by a sufficiently strong
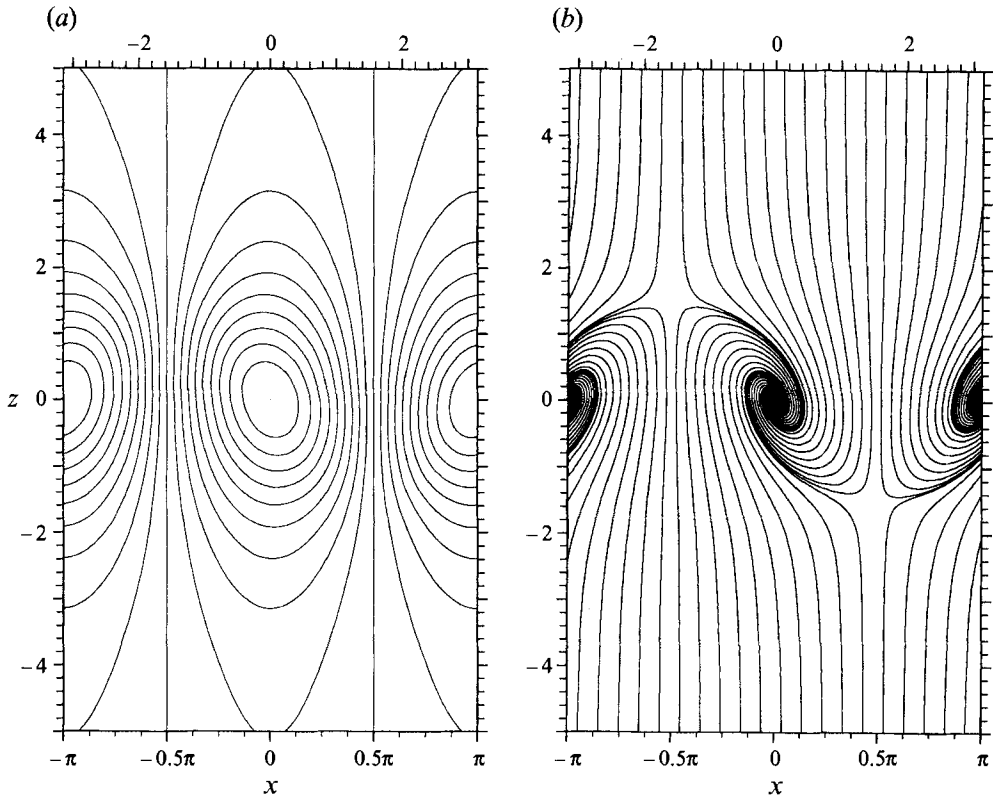
FIGURE 1. Example of periodic vortices, with amplitude 10 and $\lambda = 4$ showing (a) the perturbation streamlines (contour spacing 1), and (b) the streamlines for the whole flow projected onto the (x, z)-plane.

vorticity enhancement due to the vortex stretching, and so there is a critical strain rate below which disturbances cannot persist. This criterion can be rephrased in terms of lengthscales: for a given stagnation-point flow there is a critical vortex separation below which these vortices cannot exist.

From the above argument we can also argue that vortices can always exist unless there is some other external constraint that imposes a maximum lengthscale on the periodicity of the disturbances. In such circumstances there would ineed be a critical strain rate, below which vortices cannot exist. This is the situation found by Lagnado & Leal (1990) in their experiments in the 'four-roll mill'; although the details of their experiment and the present theory are not identical in all details, the disturbances that they observe are driven by essentially the same mechanism. They found that there was a critical strain rate in the flow driven by the 'rollers' for the existence of vortices, the axes of which were aligned with the straining flow. The form of the observed vortices is very similar to the vortices predicted in this current work.

For finite-amplitude disturbances, the nonlinear terms are no longer negligible. To find solutions for the flow field, a truncated set of equations (14)–(17) was solved numerically using a fourth-order Runge–Kutta method. Typically it was found that the magnitude of each successive mode decreases by an order of magnitude, ensuring good convergence using only a moderate number of modes. For $O(1)$ values of λ and the amplitude, accurate solutions could be found by truncating the expansions (14)–(17) after $n = 3$–6.
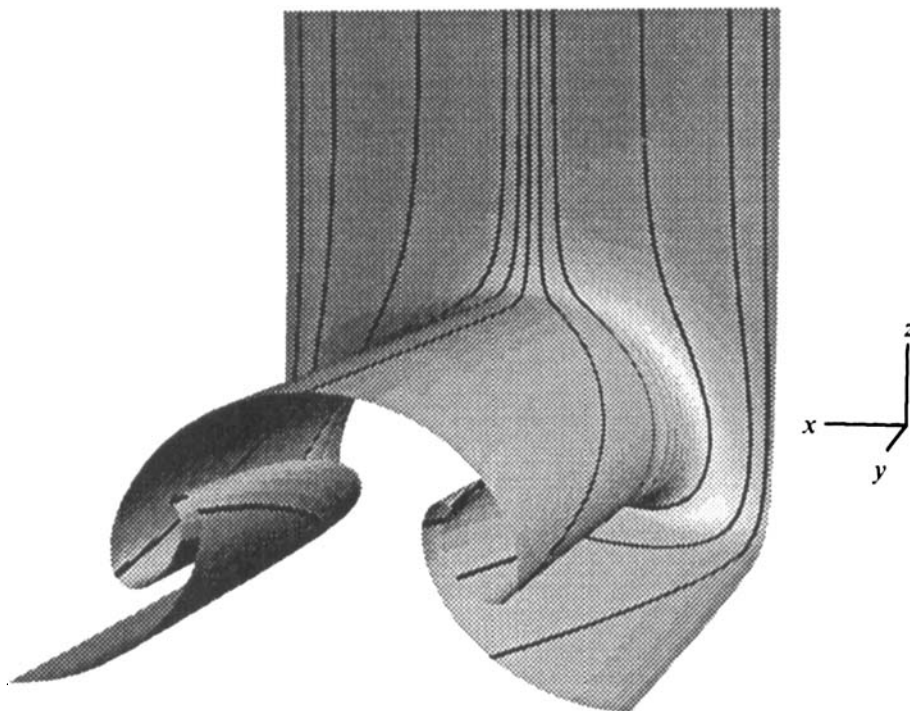
FIGURE 2. Three-dimensional representation of the total flow in a system of periodic vortices, showing how a sheet of fluid is swept into the vortices. In this example the amplitude is 10 and $\lambda = 4$. The black lines show the paths of individual fluid elements.

When looking at solutions of the governing equations we have two free parameters. The first of these, λ, is the strength of the converging flow. The second is the amplitude of the solutions. Since the condition that $\lambda > 1$ for the possible existence of non-trivial linear solutions is determined by the far-field decay of the function $a_1(z)$, where all disturbances are essentially linear, this condition will also imply the decay in the far field of this mode for the nonlinear solutions. This means that one of the boundary conditions (20) is automatically satisfied. Hence we have an extra degree of freedom which enables us to prescribe the amplitude of the perturbation vortices. We define this to be the maximum value of the stream function, which, with our assumed symmetry, will occur at the origin. Since the stream function has been nondimensionalized with respect to the kinematic viscosity, this amplitude is essentially the Reynolds number of the individual vortices.

The structure of typical periodic vortices is shown in figure 1. Figure 1(a) shows the stream function for the perturbation flow for $\lambda = 4$ where the amplitude is 10. In figure 1(b) the streamlines are shown for the total velocity components in any plane perpendicular to the y-axis. It can be seen from this diagram how the fluid flow converges towards the $z = 0$ plane and then swirls into a series of counter rotating vortices parallel with the y-axis. A three-dimensional spatial representation of this swirling motion is illustrated in figure 2, which shows the motion of a sheet of fluid as it is swept into and along the vortices; some paths of individual fluid elements are also shown. These vortices are reminiscent of the vortices found by Lagnado & Leal (1990), even though, as mentioned earlier, the details of the experimental flow are not exactly the same as the current theory. They also appear to correspond to the experimentally observed vortex in a stagnation-point flow illustrated by Aryshev *et al.* (1981).
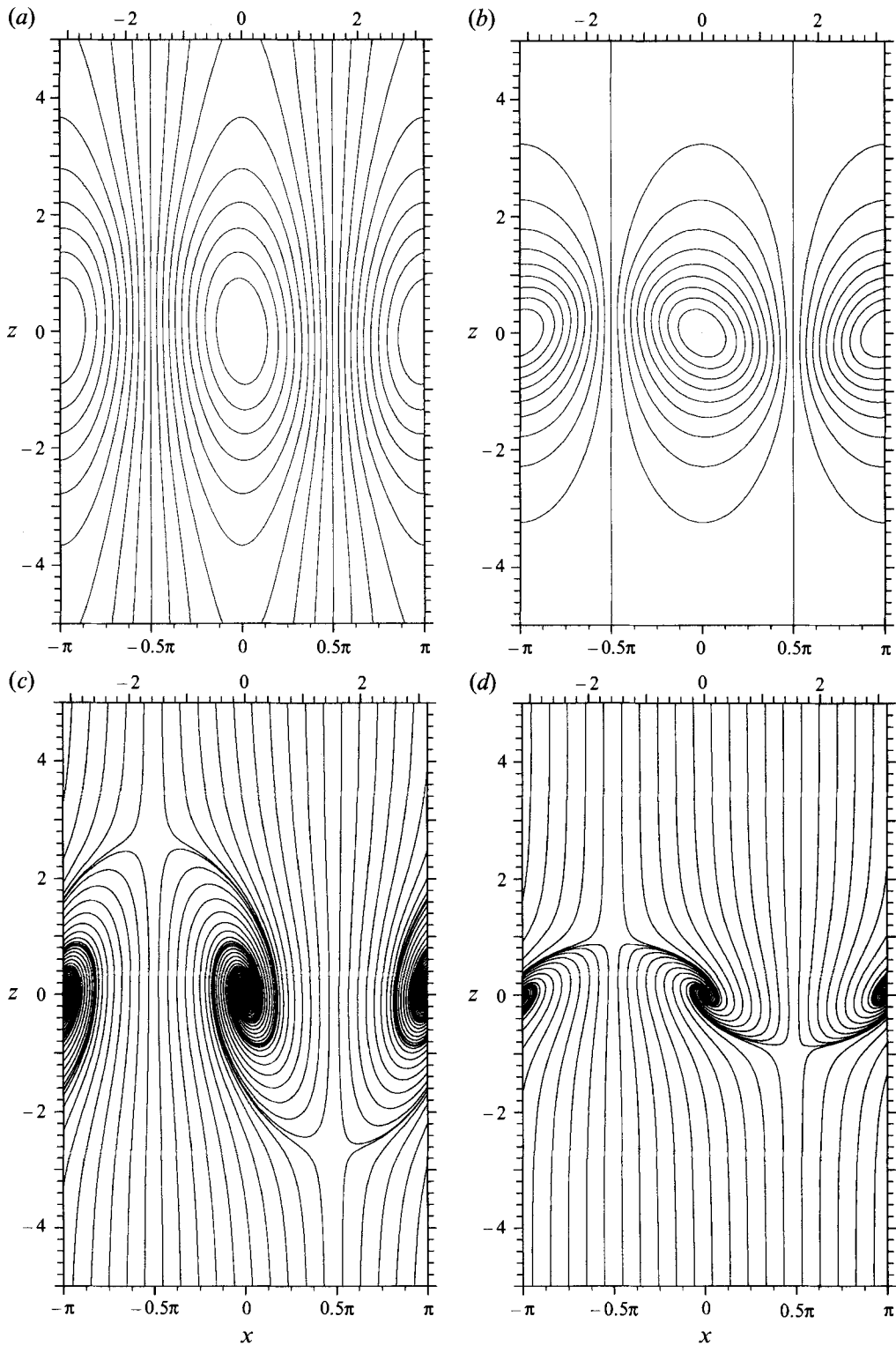
FIGURE 3. Streamlines of perturbation vortices of amplitude 10 for (*a*) $\lambda = 2$ and (*b*) $\lambda = 8$ (contour spacing 1). The corresponding streamlines for the whole flow projected into the (x, z)-plane are shown in (*c*) and (*d*).

The form that the vortices take as the strain rate, λ, is varied is illustrated in figure 3. This shows the streamlines for two other values of λ with the same amplitude 10; $\lambda = 2$ and $\lambda = 8$. For low values of λ the confining effect of the converging flow is weak, and the vortices extend further from the plane $z = 0$. As λ is increased the vortices are confined to an ever-decreasing region near this plane. For larger values of λ the streamlines of the perturbation respond with increased curvature as they cross the plane $z = 0$. This is shown in figure 4(a) for $\lambda = 36$. The perturbation vorticity is confined mainly to a region about $z = 0$ with thickness of order $\lambda^{-1/2}$, as seen in figure 4(b). The detailed structure in the large-λ limit for linear disturbances is examined in the following section.

The change in the vortices as the amplitude is varied is shown in figure 5 and 6. Initially, for low amplitudes, the perturbation stream function of the vortices is nearly symmetrical about a vertical plane through the core of the vortices, as would be expected from the linear solutions (figure 5a). As the amplitude increases, a skewness develops in this stream function (figure 5b). As the amplitude increases further the stream function tends towards a state that regains its original symmetry (figure 5c). Although this is apparent in the plots of the stream function, this trend does not manifest itself clearly in the plots of the streamlines. The streamlines corresponding to the examples in figure 5 are shown in figure 6. The most notable transition is that for low amplitudes the streamlines (figure 6a) for the total flow do not exhibit any spiral flow as such. The paths of the fluid elements are swept towards the cores of the 'vortices' without swirling around them. As a result there is a continuous wavy surface that divides the upward-flowing fluid from the downward-flowing fluid. A local analysis shows that the transition from flows that (when looked at as phase planes) have nodes at the centre of the vortices to flows that have spiral flows occurs when

$$\frac{\lambda}{2} = \left(\frac{\partial^2 \psi(0,0)}{\partial x^2} \frac{\partial^2 \psi(0,0)}{\partial z^2} \right)^{1/2} - \frac{\partial^2 \psi(0,0)}{\partial x \, \partial z}. \tag{23}$$

Thus for low amplitudes the singular points at the cores of the vortices are always nodes, and as the amplitudes increase they become foci. Equation (23) is not equivalent to the comparable criterion of H. King quoted in Lin & Corcos (1984), which as stated is incorrect. The existence of a wavy interface with nodes in the flow field was found in the experiments of Lagnado & Leal (1990). In their figure 5(d) a sinuous separation line is visible between the two incoming streams of fluid, along which there exist some nodes in the total flow, but no vortices with a full swirling motion are present.

For larger-amplitude disturbances the vortices develop a spiral flow, with the surface separating the two incoming streams of fluid wrapping itself around the vortex core. As the amplitude increases further the spiral flow eventually dominates the flow field near the plane $z = 0$.

The asymptotic form of the large-amplitude vortices is examined in §5.

4. Large-strain-rate asymptotics

The behaviour of vorticity perturbations in a converging flow with a large strain has been looked at by Neu (1984) in the context of developing a time-dependent evolution equation for the amplitude of a nonlinear spatially varying vortex sheet, and its displacement in the direction of the converging flow. His analysis is of lower precision, but enables time dependency to be taken into account. The analysis presented here goes to higher orders for the time-independent vortices that concern us, and would not be
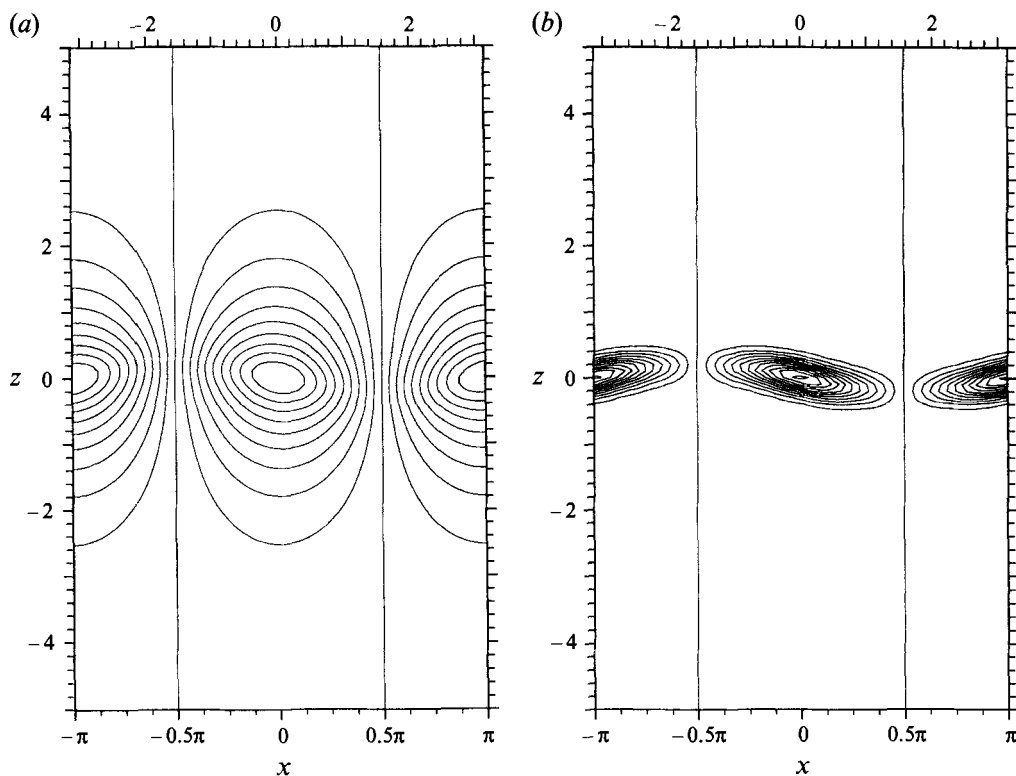
FIGURE 4. An example of vortices for a stronger strain rate in the flow, $\lambda = 36$, and amplitude 10, showing (*a*) the perturbation streamlines (contour spacing 1), and (*b*) the vorticity (contour spacing 5).

as readily extended to the time-dependent case of Neu. The decaying linear similarity solutions of Lin & Corcos (1984) are exact solutions valid for arbitrary values of λ, but do not describe the steady-state solutions of interest here.

In this section we look at the structure of the linear vortices in the limit $\lambda \to \infty$. The vortices examined will also describe the leading-order nonlinear behaviour of vortices with order-one amplitudes in this asymptotic limit. This is due to converging flow essentially confining the vorticity, at least to leading order, in a thin region near the plane $z = 0$ of thickness $\lambda^{-1/2}$. This is reminiscent of the Burgers' vortex sheet (Burgers 1948). Rescaling the governing equations by this factor in the z-direction leads to a set of equations where the nonlinear terms are of lower order than the remaining terms, and can be ignored to leading order.

Since the vortices to be considered are linear they can be represented in terms of their Fourier modes. The coefficient of each mode is then a function of z that independently satisfies

$$-\lambda z \omega' - \lambda \omega = \omega'' - n^2 \omega, \tag{24}$$

with boundary conditions

$$\psi(0) = 1, \quad \psi(z), \ \omega(z) \to 0 \quad \text{as} \quad z \to \pm \infty. \tag{26}$$

Since we are looking at linear disturbances we can choose the amplitude arbitrarily. For simplicity we make the choice that the amplitude will be 1. This is the first boundary
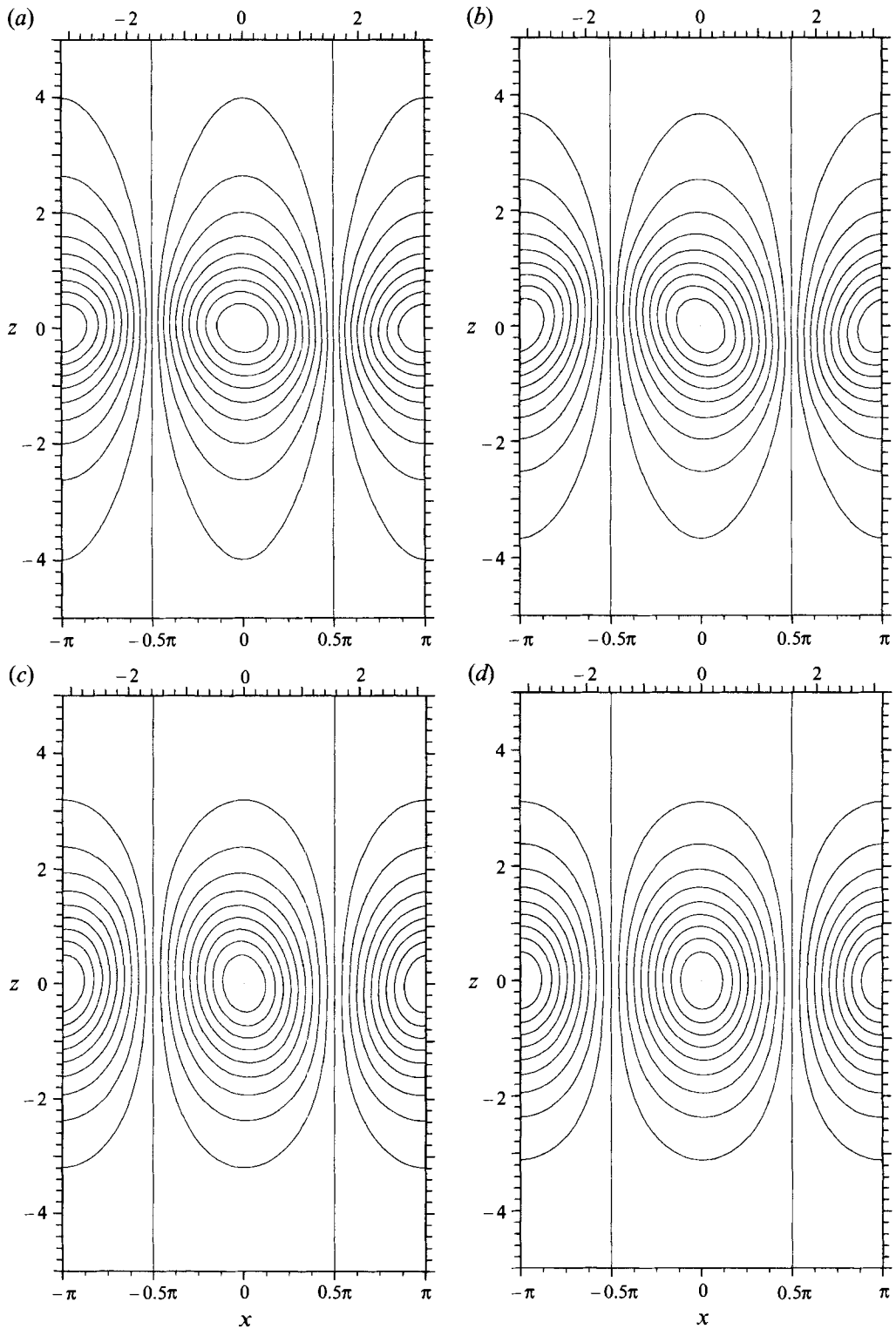
FIGURE 5. Perturbation streamlines for vortices with $\lambda = 6$ and amplitudes (*a*) 2.5 (contour spacing 0.25), (*b*) 10 (contour spacing 1), (*c*) 40 (contour spacing 4) and (*d*) 160 (contour spacing 16).

condition given in (26). In solving these equations we use the symmetry condition that requires both ψ and ω to be even functions in z. We also examine only the case $n = 1$.

An examination of these equations shows that there are two lengthscales of importance: when $z = O(1)$ and when $z = O(\lambda^{-1/2})$. Although this divides the domain into three regions the symmetry condition means that there are essentially only two regions that have to be joined together using matched asymptotic expansions.

We define an outer expansion

$$\psi(z;\lambda) = \psi_0(z) + \lambda^{-1/2}\psi_{1/2}(z) + \lambda^{-1}\psi_1(z) + \dots, \tag{27}$$

$$\omega(z;\lambda) = \omega_0(z) + \lambda^{-1/2}\omega_{1/2}(z) + \lambda^{-1}\omega_1(z) + \dots, \tag{28}$$

and an inner expansion

$$\psi(z;\lambda) = \Psi_0(\zeta) + \lambda^{-1/2}\Psi_{1/2}(\zeta) + \lambda^{-1}\Psi_1(\zeta) + \lambda^{-3/2}\Psi_{3/2}(\zeta) + \dots, \tag{29}$$

$$\omega(z;\lambda) = \lambda\Omega_0(\zeta) + \lambda^{1/2}\Omega_{1/2}(\zeta) + \Omega_1(\zeta) + \lambda^{-1/2}\Omega_{3/2}(\zeta) + \dots, \tag{30}$$

where

$$\zeta = \lambda^{1/2}z. \tag{31}$$

The leading-order inner equations are

$$-\zeta\Omega_0' - \Omega_0 = \Omega_0'', \tag{32}$$

$$\Psi_0'' = -\Omega_0. \tag{33}$$

The general solution to (32) is

$$\Omega_0(\zeta) = A_0 e^{-\zeta^2/2} \int_0^\zeta e^{\zeta'^2/2} \, d\zeta' + B_0 e^{-\zeta^2/2}. \tag{34}$$

The condition that $\Omega_0(\zeta)$ is an even function tells us that $A_0 = 0$. Using this we can then find the solution to the stream-function equation (33):

$$\Psi_0(z) = -B_0 \int_0^\zeta \int_0^{\zeta'} e^{-\zeta''^2/2} \, d\zeta'' \, d\zeta' + C_0\zeta + D_0. \tag{35}$$

Again the condition that the solutions are even functions gives $C_0 = 0$. The choice that the amplitude is 1 yields $D_0 = 1$.

At $O(\lambda^{-1/2})$ the equations are essentially the same, and hence the solutions will be similar, the only difference being that $D_{1/2} = 0$. At $O(\lambda^{-1})$ the equations are

$$\Omega_1'' + \zeta\Omega_1' + \Omega_1 = \Omega_0 = B_0 e^{-\zeta^2/2}, \tag{36}$$

$$\Psi_1'' = -\Omega_1 + \Psi_0. \tag{37}$$

The even solution to (36) is

$$\Omega_1 = B_1 e^{-\zeta^2/2} + B_0 e^{-\zeta^2/2} \int_0^\zeta e^{\zeta'^2/2} \int_0^{\zeta'} e^{-\zeta''^2/2} \, d\zeta'' \, d\zeta'. \tag{38}$$

Similarly the next-order solution is

$$\Omega_{3/2} = B_{3/2} e^{-\zeta^2/2} + B_{1/2} e^{-\zeta^2/2} \int_0^\zeta e^{\zeta'^2/2} \int_0^{\zeta'} e^{-\zeta''^2/2} \, d\zeta'' \, d\zeta'. \tag{39}$$
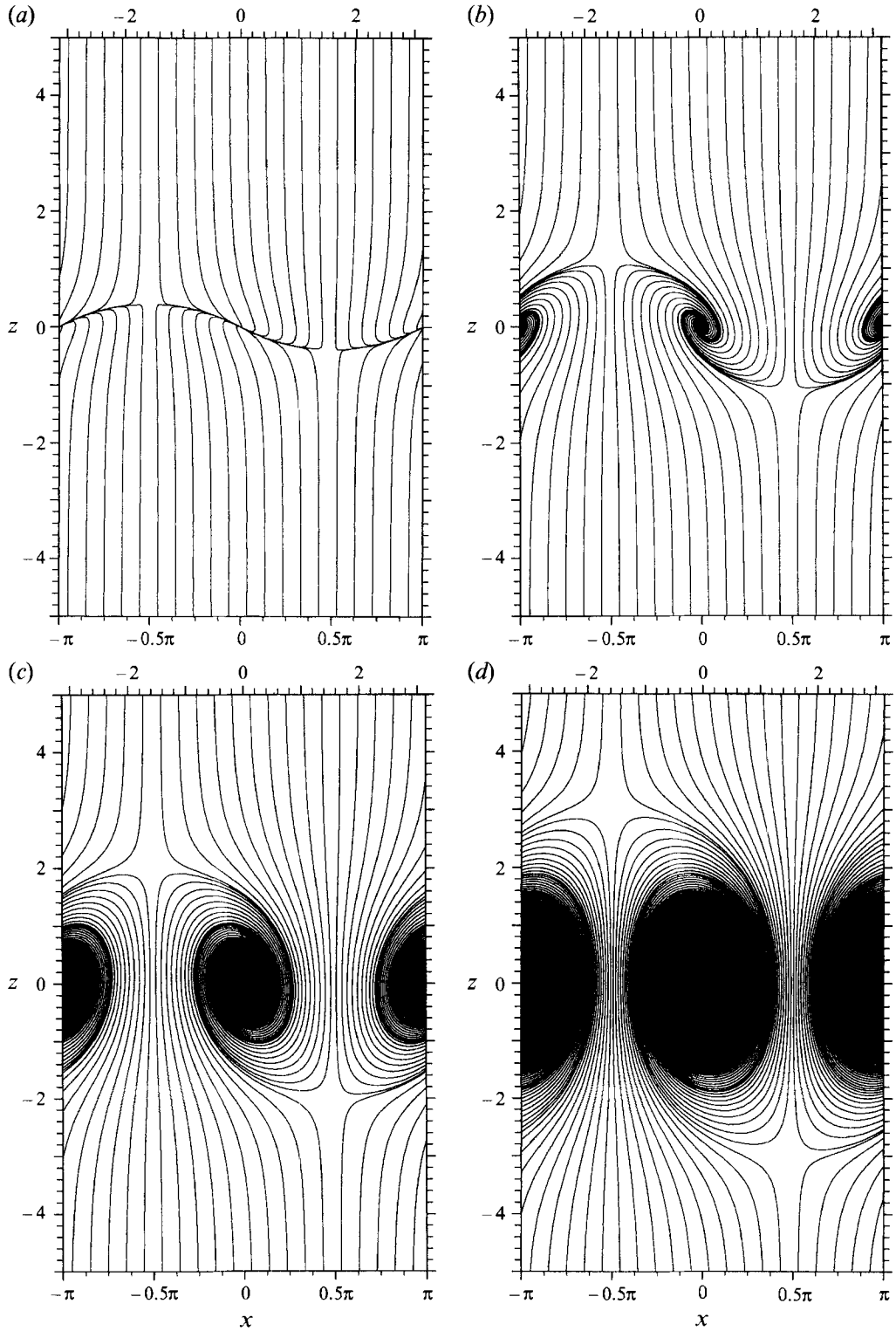
FIGURE 6. Streamlines of the whole flow projected onto the (x, z)-plane corresponding to the finite-amplitude vortices shown in figure 5, with amplitudes (a) 2.5, (b) 10, (c) 40 and (d) 160.

The corresponding solutions for the stream function are

$$\Psi_1 = \frac{\zeta^2}{2} - B_1 \int_0^\zeta \int_0^{\zeta'} e^{-\zeta''^2/2} \, d\zeta'' \, d\zeta'$$

$$- B_0 \Bigg(\int_0^\zeta \int_0^{\zeta'} \int_0^{\zeta''} \int_0^{\zeta'''} e^{-\zeta''''^2/2} \, d\zeta'''' \, d\zeta''' \, d\zeta'' \, d\zeta'$$

$$+ \int_0^\zeta \int_0^{\zeta'} e^{-\zeta'^2/2} \int_0^{\zeta''} e^{\zeta''^2/2} \int_0^{\zeta'''} e^{-\zeta'''^2/2} \, d\zeta'''' \, d\zeta''' \, d\zeta'' \, d\zeta' \Bigg) \tag{40}$$

and

$$\Psi_{3/2} = - B_{3/2} \int_0^\zeta \int_0^{\zeta'} e^{-\zeta''^2/2} \, d\zeta'' \, d\zeta'$$

$$- B_{1/2} \Bigg(\int_0^\zeta \int_0^{\zeta'} \int_0^{\zeta''} \int_0^{\zeta'''} e^{-\zeta'''^2/2} \, d\zeta'''' \, d\zeta''' \, d\zeta'' \, d\zeta'$$

$$+ \int_0^\zeta \int_0^{\zeta'} e^{-\zeta'^2/2} \int_0^{\zeta''} e^{-\zeta''^2/2} \int_0^{\zeta'''} e^{-\zeta'''^2/2} \, d\zeta'''' \, d\zeta''' \, d\zeta'' \, d\zeta' \Bigg). \tag{41}$$

Higher-order terms could be found in a similar fashion.

In the outer region the leading order equations are

$$z\omega_0' - \omega_0 = 0, \tag{42}$$

$$\psi_0'' - \psi_0 = -\omega_0. \tag{43}$$

The vorticity equation (42) has the solution

$$\omega_0 = a_0/z. \tag{44}$$

At the next two orders the solutions are

$$\omega_{1/2} = a_{1/2}/z, \tag{45}$$

$$\omega_1 = a_1/z + a_0/z^3 + (a_0 \log z)/z. \tag{46}$$

In order to be able to match these solutions to the inner solutions it is necessary that either the large-ζ asymptotic behaviour of some Ω_i must have a ζ^{-1} term, or that the constants, a_i, are zero. Potentially a ζ^{-1} contribution from an Ω_i first occurs from the integral term in (38). This contribution would only be able to match with the outer term $\omega_{1/2}$. Hence the z^{-1} term in ω_0 cannot be matched with any term in the inner solutions and we have

$$a_0 = 0. \tag{47}$$

Knowing this, the corresponding solutions in the stream-function expansion are

$$\psi_0 = b_0 e^{-z}, \tag{48}$$

$$\psi_{1/2} = -\tfrac{1}{2}a_{1/2}(\text{Ei}(-z) e^z - \text{Ei}(z) e^{-z}) + b_{1/2} e^{-z}, \tag{49}$$

$$\psi_1 = -\tfrac{1}{2}a_1(\text{Ei}(-z) e^z - \text{Ei}(z) e^{-z}) + b_1 e^{-z}, \tag{50}$$

for some constants b_i. Here $\text{Ei}(z)$ is the exponential integral function (see Abramowitz & Stegun 1964).

In order to match the stream functions in the two regions we have to find the large-ζ behaviour of the double integral in (35). This double integral can be re-expressed as

$$\int_0^\zeta \int_0^{\zeta'} e^{-\zeta''^2/2} \, d\zeta'' \, d\zeta' = \left(\frac{\pi}{2}\right)^{1/2} \zeta - 1 + (\pi)^{1/2} \mathrm{i}^1 \, \text{erfc}\left(\frac{\zeta}{2^{1/2}}\right), \tag{51}$$

where $\mathrm{i}^1 \text{erfc}$ is the first integral of the complementary error function (see Abramowitz & Stegun 1964). For large ζ this term decays as $z^{-2} e^{-\zeta^2/2}$ and as such plays no role in the matching process.
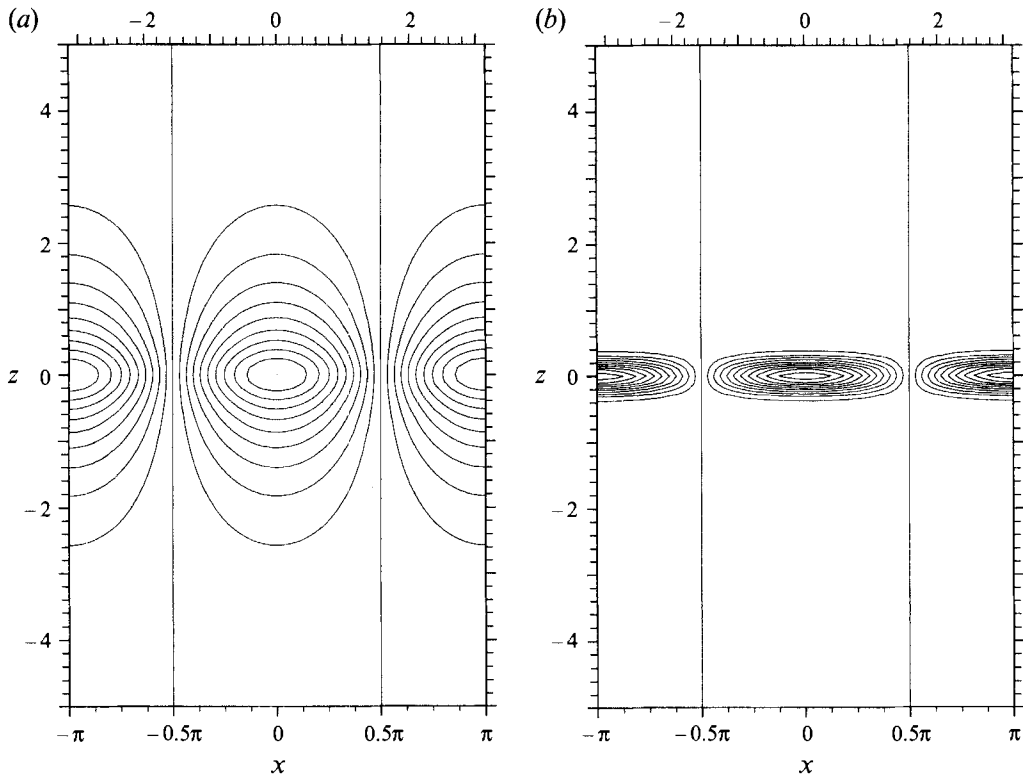
FIGURE 7. The (*a*) stream function and (*b*) vorticity distribution predicted by the large-λ asymptotic theory for $\lambda = 36$. This is virtually indistinguishable from the full solution for $\lambda = 36$ and amplitude 1.

Matching with the inner solutions using Van Dykes' matching rules gives

$$B_0 = 0, \quad B_{1/2} = (2/\pi)^{1/2}, \quad B_1 = 2/\pi, \tag{52}$$

$$b_0 = 1, \quad b_{1/2} = (2/\pi)^{1/2}, \quad b_1 = 2/\pi, \tag{53}$$

and

$$a_0 = 0, \quad a_{1/2} = 0, \quad a_1 = 1. \tag{54}$$

In order to be able to determine the value of $B_{3/2}$ the second-order large-ζ asymptotic behaviour of the second quadruple integral in (41) needs to be found. This term, which grows as ζ, has not yet been determined.

With these results a composite expansion can be formed for ψ, using only the first three terms in both the inner and outer expansions:

$$\psi(z;\lambda) \approx e^{-z} + \lambda^{-1/2} \left(\frac{2}{\pi}\right)^{1/2} e^{-z} + \lambda^{-1} \frac{2}{\pi} e^{-z} - \lambda^{-1} \tfrac{1}{2} (\text{Ei}(-z) e^z - \text{Ei}(z) e^{-z})$$

$$- \lambda^{-1/2} 2^{1/2} i^1 \text{erfc}\left(\frac{\lambda^{1/2} z}{2^{1/2}}\right) - \lambda^{-1} \frac{2}{\pi^{1/2}} i^1 \text{erfc}\left(\frac{\lambda^{1/2} z}{2^{1/2}}\right). \tag{55}$$

If the contours for this approximation are plotted for $\lambda = 36$ (figure 7) the results are virtually indistinguishable from those that are obtained by solving the full nonlinear problem with amplitude 1, with the differences not visible in the plots presented here.

The analysis of this section reveals the essential difference between the decaying similarity solution of Lin & Corcos and the steady-state solutions that are the concern

of this work. To derive their similarity solutions they have to impose a Gaussian vorticity distribution. This is the same as the leading-order vorticity found here, and hence plots of the respective solutions will appear similar. However, in this large-λ limit the Gaussian distribution of vorticity is not the exact distribution found here. In particular, the non-zero value of a_1 means that there is a weak relatively slowly decaying component to the vorticity that penetrates into the outer region that is excluded by the form of the similarity solution. It is the enhancement of this vorticity by vortex stretching in this outer region that enables the disturbances to survive despite the dissipation due to viscosity.

5. Large-amplitude asymptotics

In this section we examine the form that the vortices take in the asymptotic limit of large amplitude. Although Neu (1984) considered a model for the large-amplitude limit for 'collapsed vortices' he made some assumptions that do not hold up to detailed examination. He assumed that the vortices could be considered in isolation and taken to be approximately circular. The assumption that the vortex was circular was a reasonable approximation for the vortex found in his numerical simulation; however, this is not always the case. For instance the vortices found here for lower values of λ are distinctly elongated in the z-direction. However, it is a reasonable approximation for larger values of λ. The other assumption, that the vortices could be considered in isolation is not strictly valid if one is looking for a steady-state solution. Robinson & Saffman (1984) showed that steady single vortices could not exist in the stagnation-point flow considered here, but only in stagnation-point flows where there was an additional non-zero component of the converging flow, however weak, coming in along the x-axis. However Moffatt, Kida & Ohkitani (1994) have re-examined this problem, and have shown that although the solutions of Neu are not steady, the lateral leakage of vorticity is asymptotically small, even if there is a small lateral *diverging* component to the flow, and so the vortices can be approximated as being steady. The model of Neu will be a valid approximation for larger values of λ. By retaining the periodicity we do not have to make an approximation of a steady flow as the vorticity that diffuses laterally out of any single vortex will be cancelled by vorticity of the opposite sign diffusing out of its neighbour, and so the confining effect on the vorticity of the extra converging component of the background flow that is required for a steady state for a single vortex is not required here. In addition we make no *a priori* assumptions about the exact shape of the vortices, and so this analysis does not require large values of λ.

If we let the amplitude of the vortices be μ, then we can rescale (9) and (10) to give

$$-\frac{\partial \psi^\dagger}{\partial z}\frac{\partial \omega^\dagger}{\partial x} + \frac{\partial \psi^\dagger}{\partial x}\frac{\partial \omega^\dagger}{\partial z} = \mu^{-1}\left(\lambda z\frac{\partial \omega^\dagger}{\partial z} + \lambda\omega^\dagger + \left(\frac{\partial^2}{\partial x^2} + \frac{\partial^2}{\partial z^2}\right)\omega^\dagger\right), \tag{56}$$

$$\omega^\dagger = -\left(\frac{\partial^2}{\partial x^2} + \frac{\partial^2}{\partial z^2}\right)\psi^\dagger, \tag{57}$$

where $\qquad\qquad \mu\omega^\dagger = \omega \quad \text{and} \quad \mu\psi^\dagger = \psi. \tag{58}$

From the leading-order behaviour of (56),

$$-\frac{\partial \psi^\dagger}{\partial z}\frac{\partial \omega^\dagger}{\partial x} + \frac{\partial \psi^\dagger}{\partial x}\frac{\partial \omega^\dagger}{\partial z} = 0, \tag{59}$$
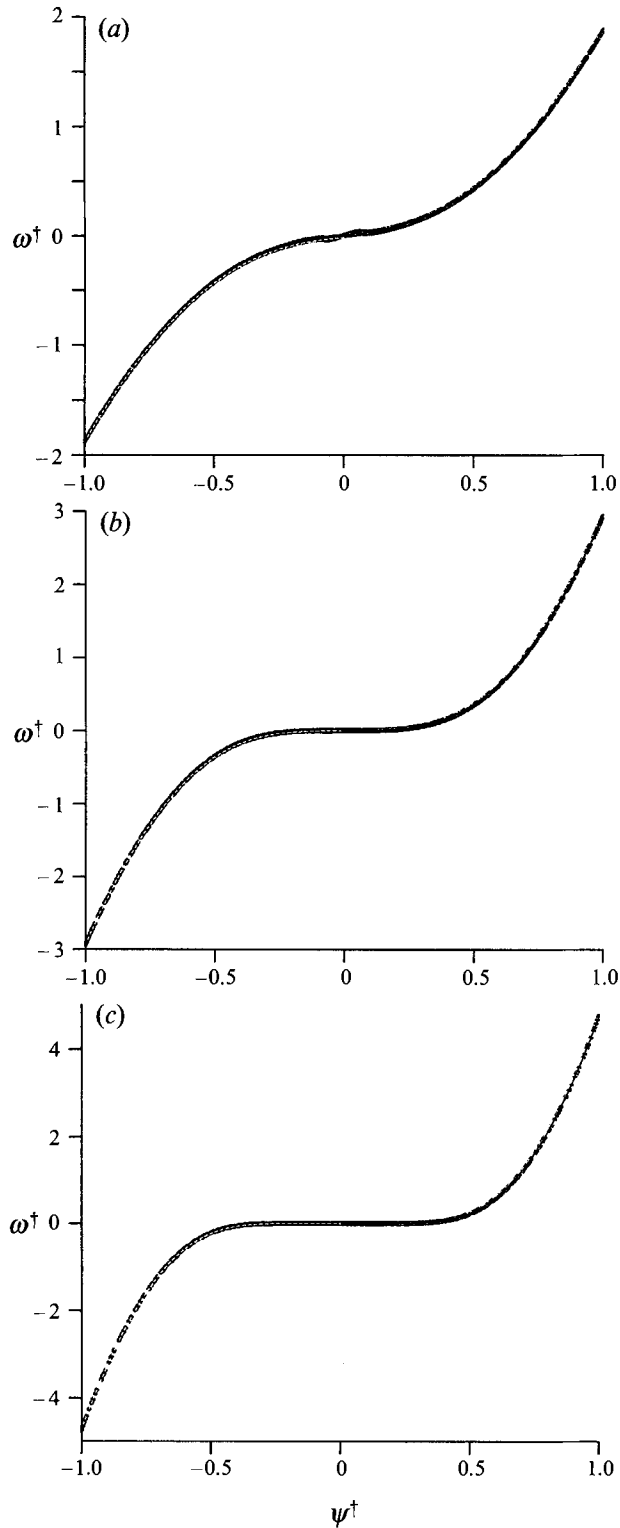
FIGURE 8. Scatter plots of $\omega^\dagger$ versus $\psi^\dagger$ for vortices of amplitude 400, with (a) $\lambda = 4$, (b) $\lambda = 8$ and (c) $\lambda = 16$. Superimposed on these for $\psi^\dagger > 0$ are the numerical calculations for the corresponding functions $g(\psi^\dagger)$, and for $\psi^\dagger < 0$ the corresponding relationship for a Burgers vortex.

we see that $\psi^\dagger$ and $\omega^\dagger$ will have some functional relationship of the form

$$\omega^\dagger = g(\psi^\dagger) \tag{60}$$

for some as yet unknown function $g(\cdot)$. Such a relationship can be verified by examining solutions found by solving (14)–(17) to find ψ and ω for some large amplitude (say, $\mu = 400$). If the rescaled values of ψ and ω evaluated at the vertices of any grid (such as that used for the contour plots in previous figures) are then plotted on a scatter diagram, it can be seen that all of the points lie close to a single curve (see figure 8).

Further information can be extracted from the vorticity equation by integrating (56) over any area, S_ψ, bounded by a closed streamline, C_ψ. Since the perturbation velocity is divergence free it is straightforward to show that such an integral of the left-hand side of (56) is identically zero, leaving the exact identity

$$0 = \lambda \int_{S_\psi} \left(z \frac{\partial \omega^\dagger}{\partial z} + \omega^\dagger \right) dS + \int_{S_\psi} \nabla^2 \omega^\dagger \, dS. \tag{61}$$

By re-expressing the first integral as a double integral in x and z, and integrating by parts, we find

$$\int_{S_\psi} \left(z \frac{\partial \omega^\dagger}{\partial z} + \omega^\dagger \right) dS = \int_{x_{\psi-}}^{x_{\psi+}} \left[z \omega^\dagger \right]_{z_{\psi-}(x)}^{z_{\psi+}(x)} dx, \tag{62}$$

where $x_{\psi\pm}$ and $z_{\psi\pm}(x)$ are the appropriate limits for the closed streamline. Note that inside the integral we are evaluating $\omega^\dagger$ on the streamline, hence it will take the value $g(\psi^\dagger)$ to leading order in the limit $\mu \to \infty$. As this is a constant around the streamline, it can be taken outside the integral. The remaining integral is simply the area enclosed by the streamline. This method essentially uses the techniques of the Prandtl–Batchelor theorem (Batchelor 1956).

We can also simplify the second integral by the use of the divergence theorem

$$\int_{S_\psi} \nabla^2 \omega^\dagger \, dS = \int_{C_\psi} \hat{\boldsymbol{n}} \cdot \nabla \omega^\dagger \, dl \approx \int_{C_\psi} g'(\psi^\dagger) \, \hat{\boldsymbol{n}} \cdot \nabla \psi^\dagger \, dl. \tag{63}$$

Again, to leading order, we can extract the $g'(\psi^\dagger)$ term from inside the integral, and use the divergence theorem again to give

$$0 = \lambda g(\psi^\dagger) A(\psi^\dagger) + g'(\psi^\dagger) \int_{S_\psi} g(\psi^\dagger) \, dS, \tag{64}$$

where $A(\psi^\dagger)$ is the area enclosed by the streamline.

Equation (64), when combined with the stream-function equation and the periodicity, is almost sufficient to define the problem. It is fully defined when we recall that the rescaling by the amplitude, μ, gives the requirement that $\psi^\dagger$ takes the value 1 at the origin. These equations were solved numerically using an iterative procedure to find $\psi^\dagger(x, z)$ and $g(\cdot)$. First (57) was re-expressed in terms of an integral equation using the periodic Green's function:

$$\psi_n^\dagger(x, z) = \int_0^{2\pi} \int_{-\infty}^{\infty} G(x, z, x', z') \, g_n(\psi^\dagger(x', z')) \, dz' \, dx', \tag{65}$$

where
$$G(x, z, x', z') = -\frac{1}{4\pi} \log \left(\cosh(z - z') - \cos(x - x') \right). \tag{66}$$

For a given function $g_n(\cdot)$, this integral was discretized over a grid to give a system of equations that were solved to find $\psi_n^\dagger(x, z)$ using NAG library routines. Reasonable accuracy could be achieved by the use of a limited range in the z-direction because the vorticity was found to decay rapidly with increasing $|z|$. Further simplification was possible by using the symmetries of the problem, which meant that the integral needed only to be evaluated over a quarter of a vortex cell, thus reducing the computational domain by a factor of 8. The solution found could then be used to find an updated version of the function g_{n+1} (to within a multiplicative constant) using the ordinary differential equation

$$0 = \lambda g_{n+1}(\psi^\dagger) A(\psi^\dagger) + g'_{n+1}(\psi^\dagger) \int_{S_\psi} g_n(\psi^\dagger) \, \mathrm{d}S. \tag{67}$$

This could then be used to calculate an updated version of $\psi_{n+1}^\dagger$ where the condition that $\psi(0, 0) = 1$ yields the multiplicative constant for g_{n+1}. This iterative procedure converges to give both $\psi^\dagger$ and $g(\cdot)$ for asymptotically large-amplitude disturbances. The curves $g(\psi^\dagger)$ for $\lambda = 4, 8, 16$ are superimposed on the scatter plots in figure 8, showing good agreement.

When the corresponding curves $g(\psi)$ for a Burgers vortex with the same maximum value of the vorticity is superimposed on one half of these graphs they are found to be virtually indistinguishable from those calculated here for $\lambda = 6$ and 8, with only small differences visible for $\lambda = 4$ (see figure 8). However, for these lower values of λ the streamlines are not circular as in the axisymmetric Burgers vortex, or as in the asymptotic limit found by Moffatt *et al.* (1994) for a quasi-steady vortex in the extensional flow considered here. As λ increases this similarity would be expected, as the external flow confines the vortices ever closer to the plane $z = 0$, and so they are free to take up this circular configuration. Why the agreement nevertheless holds so well for the lower values of λ is not clear.

6. Conclusion

In this paper we have found a new class of steady-state three-dimensional nonlinear solutions to the Navier–Stokes equation. These consist of a periodic array of counter-rotating vortices lying in a plane of symmetry in a stagnation-point flow, with the axes of the vortices aligned with the diverging component of the flow. The only previously known flows that are steady-state perturbations to the stagnation-point flow, and that are solutions to the Navier–Stokes equation, are the Burgers vortex sheet (Burgers 1984) and the single Fourier mode solution of Craik & Criminale (1986). We feel that the existence of these solutions to the Navier–Stokes equation is of both intrinsic and practical interest. They lead to a clearer interpretation of experimental results such as those of Lagnado & Leal (1990) and Aryshev *et al.* (1981). We have been able to show that the presence of vortices and of a wavy surface of separation between the incoming streams in the 'four-roll mill' experiment are different manifestations of the same type of phenomenon, the former simply corresponding to a larger-amplitude perturbation than the latter. The time-dependent numerical analysis of Lin & Corcos (1984) indicates that, under certain restrictions such as periodicity, these structures may well be stable. We have only considered steady-state vortices here. A more general time-dependent analysis may be able to provide a relationship between an initial vorticity distribution and the final amplitude of the vortices, as is possible with the Burgers vortex.

REFERENCES

ABRAMOWITZ, M. & STEGUN, I. A. 1964 *Handbook of Mathematical Functions.* Dover.

ARYSHEV, YU. A., GOLOVIN, V. A. & ERSHIN, SH. A. 1981 Stability of colliding flows. *Fluid Dyn.* **16**, 755–759.

BATCHELOR, G. K. 1956 On steady laminar flow with closed streamlines at large Reynolds number. *J. Fluid Mech.* **1**, 177–191.

BURGERS, J. M. 1948 A mathematical model illustrating the theory of turbulence. *Adv. Appl. Mech.* **1**, 171–199.

CORCOS, G. M. & LIN, S. J. 1974 The mixing layer: deterministic models of a turbulent flow. Part 2. The origin of the three dimensional motion. *J. Fluid Mech.* **139**, 67–95.

CRAIK, A. D. D. & CRIMINALE, W. O. 1986 Evolution of wavelike disturbances in shear flows: a class of exact solutions of the Navier–Stokes equations. *Proc. R. Soc. Lond.* A **406**, 13–26.

KNIO, O. M. & GHONIEM, A. F. 1992 The three-dimensional structure of periodic vorticity layers under non-symmetric conditions. *J. Fluid Mech.* **243**, 353–392.

LAGNADO, R. R. & LEAL, L. G. 1990 Visualization of three-dimensional flow in a four-roll mill. *Exps. Fluids* **9**, 25–32.

LAGNADO, R. R., PHAN-THIEN, N. & LEAL, L. G. 1984 The stability of two-dimensional linear flows. *Phys. Fluids* **27**, 1094–1101.

LASHERAS, J. C., CHO, J. S. & MAXWORTHY, T. 1986 On the origin and evolution of streamwise vortical structures in a plane, free shear layer. *J. Fluid Mech.* **172**, 231–258.

LASHERAS, J. C. & CHOI, H. 1988 Three-dimensional instability of a plane shear layer: an experimental study of the formation and evolution of streamwise vortices. *J. Fluid Mech.* **189**, 53–86.

LIN, S. J. & CORCOS, G. M. 1984 The mixing layer: deterministic models of a turbulent flow. Part 3. The effect of plane strain on the dynamics of streamwise vortices. *J. Fluid Mech.* **141**, 139–178.

MEIBURG, E. & LASHERAS, J. C. 1988 Experimental and numerical investigation of the three-dimensional transition in plane wakes. *J. Fluid Mech.* **190**, 1–37.

METCALFE, R. W., ORSZAG, S. A., BRACHET, M. E., MENON, S. & RILEY, J. J. 1987 Secondary instability of a temporally growing mixing layer. *J. Fluid Mech.* **184**, 207–243.

MOFFATT, H. K., KIDA, S. & OHKITANI, K. 1994 Stretched vortices – the sinews of turbulence: High Reynolds number asymptotics. *J. Fluid Mech.* **259**, 241–264.

MOSER, R. D. & ROGERS, M. M. 1991 Mixing transition and the cascade to small scales in a plane mixing layer. *Phys. Fluids* A **3**, 1128–1134.

NEU, J. C. 1984 The dynamics of stretched vortices. *J. Fluid Mech.* **143**, 253–276.

PEARSON, J. R. A. 1959 The effect of uniform distortion on weak homogeneous turbulence. *J. Fluid Mech.* **5**, 274–288.

ROBINSON, C. & SAFFMAN, P. G. 1984 Stability and structure of stretched vortices. *Stud. Appl. Maths* **70**, 163–181.

TAYLOR, G. I. 1934 The formation of emulsions in definable fields of flow. *Proc. R. Soc. Lond.* A **146**, 501–523.